

Comparing Euclidean and Hyperbolic K-Means for Generalized Category Discovery

Mohamad Dalal¹ ^a, Thomas B. Moeslund^{1,2} ^b, and Joakim Bruslund Haurum^{2,3} ^c

¹*Visual Analysis and Perception Lab, Aalborg University, Aalborg, Denmark*

²*Pioneer Centre for AI, Denmark*, ³*Center for Software Technology, University of Southern Denmark, Vejle, Denmark*
 {moda, tbm}@create.aau.dk, jhau@mmti.sdu.dk

Keywords: Generalized Category Discovery, Hyperbolic Representation Learning, Hyperbolic K-Means

Abstract: Hyperbolic representation learning has been widely used to extract implicit hierarchies within data, and recently it has found its way to the open-world classification task of Generalized Category Discovery (GCD). However, prior hyperbolic GCD methods only use hyperbolic geometry for representation learning and transform back to Euclidean geometry when clustering. We hypothesize this is suboptimal. Therefore, we present Hyperbolic Clustered GCD (HC-GCD), which learns embeddings in the Lorentz Hyperboloid model of hyperbolic geometry, and clusters these embeddings directly in hyperbolic space using a hyperbolic K-Means algorithm. We test our model on the Semantic Shift Benchmark datasets, and demonstrate that HC-GCD is on par with the previous state-of-the-art hyperbolic GCD method. Furthermore, we show that using hyperbolic K-Means leads to better accuracy than Euclidean K-Means. We carry out ablation studies showing that clipping the norm of the Euclidean embeddings leads to decreased accuracy in clustering unseen classes, and increased accuracy for seen classes, while the overall accuracy is dataset dependent. We also show that using hyperbolic K-Means leads to more consistent clusters when varying the label granularity.

1 INTRODUCTION

Image classification has seen a renascence in recent years, with a shift in focus onto open-world classification. One such task is Generalized Category Discovery (GCD) (Vaze et al., 2022a), which poses the challenge of being able to cluster seen and unseen classes simultaneously.

One approach to better classify unseen classes is to utilize the latent hierarchies present within the data, as hierarchies are implicitly present in most data (Ge et al., 2023; Hsu et al., 2021). Hyperbolic representation learning is often used to learn these hierarchies, and recently some works have explored the use of hyperbolic representation learning to solve the GCD task (Liu et al., 2025a; Rathore et al., 2025).

However, all hyperbolic learned non-parametric methods resort to performing clustering on the Euclidean embeddings instead of hyperbolic (Liu et al., 2025a; Rathore et al., 2025). This can lead to distortion of the learned hierarchies, as Euclidean geometry is not optimal for representing these hierarchies (Gromov, 1987). This work aims to explore clustering directly in hyperbolic geometry, by introducing a hyperbolic K-Means algorithm and testing its performance on the Semantic Shift Benchmark (Vaze et al., 2022b), the most common GCD benchmark.

To achieve this we introduce Hyperbolic Clustered GCD (HC-GCD), which is a GCD model trained using contrastive learning in the Lorentz Hyperboloid model of hyperbolic geometry. This was chosen instead of the Poincaré model due to the existence of a closed form centroid, which is later used to create clusters using a hyperbolic adaptation of the semi-supervised K-Means algorithm, seen in Figure 1.¹

Our contributions are as follows:

- Creating a hyperbolic K-Means algorithm, and showing its benefits on the GCD task.
- Mathematically proving that the Einstein Mid-point is equivalent to the Lorentz Centroid.
- Demonstrating that hyperbolic clustering leads to better implicit feature hierarchies, through a label granularity analysis.

^a <https://orcid.org/0009-0006-3857-4220>
^b <https://orcid.org/0000-0001-7584-5209>
^c <https://orcid.org/0000-0002-0544-0422>

¹The code for this paper can be found at <https://github.com/MohamadDalal/HC-GCD>

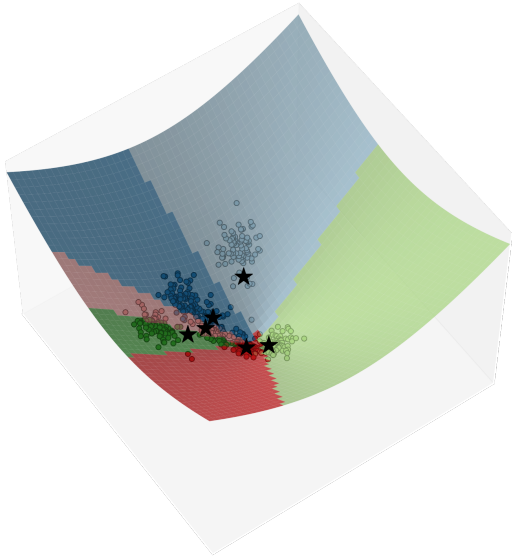


Figure 1: Hyperbolic semi-supervised K-Means in the Lorentz Hyperboloid model of hyperbolic geometry. The centroids are represented as black stars.

2 RELATED WORKS

Hyperbolic Representation Learning Hyperbolic geometry is the geometry of surfaces with constant negative Gaussian curvature. This is in contrast to Euclidean geometry for surfaces with zero Gaussian curvature and hyperspherical geometry for surfaces with constant positive Gaussian curvature (Ratcliffe et al., 1994). This leads to differing properties, such as the existence of at least two lines parallel to a stationary line in contrast to a maximum of one in Euclidean geometry, and the exponential growth of areas of spheres in contrast to polynomial growth in Euclidean geometry (Krioukov et al., 2010). This exponential growth makes hyperbolic geometry particularly suitable for representing hierarchies, which also grow exponentially with increased depth (Gromov, 1987). Hyperbolic geometry can be represented by many different models. However, the three most common are the Poincaré Hypersphere, the Klein Hypersphere and the Lorentz Hyperboloid.

Hyperbolic geometry’s affinity to representing hierarchies led to it being explored for learning representations of many types of hierarchical data. An example from the text domain is skip-gram by Leimeister and Wilson (2018), where they generate hyperbolic text embeddings by adding a hyperbolic distance objective to Word2Vec (Mikolov et al., 2013). While from the vision domain Ge et al. (2023) learn the hierarchies between scenes and the objects within them, while Atigh et al. (2022) and Suris et al. (2021) use the norm of hyperbolic embeddings to calculate

the uncertainty of predictions. These methods are built upon a Euclidean backbone where the final features are lifted into hyperbolic geometry using the exponential map. There has, however, also been recent work on making fully hyperbolic neural networks (van Spengler et al., 2023). In the intersection of the two modalities is MERU (Desai et al., 2023), which learns vision-text embeddings in the Lorentz Hyperboloid model of hyperbolic geometry. This is done using hyperbolic distance contrastive loss and hyperbolic entailment loss to learn the hierarchy present between an image and its textual description.

More details can be found in the surveys by Peng et al. (2022), and Mettes et al. (2024).

Generalized Category Discovery In 2022 Vaze et al. (2022a) proposed the *Generalized Category Discovery* task, where a mix of labeled and unlabeled data has to be clustered according to both seen and unseen classes. Vaze et al. (2022a) originally proposed a two stage approach consisting of a representation learning step (self-supervised contrastive and supervised contrastive learning) followed by a clustering step achieved through a semi-supervised K-Means algorithm. Subsequent approaches investigating alternative approaches such as parametric classification (Wen et al., 2023), hierarchical K-Means and self-expertise (Rastegar et al., 2024), spatial prompt tuning (Wang et al., 2024), Gaussian Mixture Models (Zhao et al., 2023), student-teacher distillation (Vaze et al., 2023), etc. An in-depth review of the Category Discovery fields was conducted by He et al. (2025a).

There has throughout the GCD research field been an interest in leveraging the underlying hierarchical structure of the dataset in various ways. The SelEx (Rastegar et al., 2024) method constructed hierarchies through a balanced K-Means approach, SEAL (He et al., 2025b) proposed a semantic-aware hierarchical learning approach, while InfoSieve (Rastegar et al., 2023) constructed an implicit hierarchy based through an information theoretic lens. More recently, two approaches have been proposed which adapt hyperbolic geometry. Firstly, HIDISC (Rathore et al., 2025) was proposed as a hyperbolic approach for the sub-task of Domain Generalization based on applying CutMix (Yun et al., 2019) in the tangent space, Busemann Learning (Ghadimi Atigh et al., 2021) and hyperbolic contrastive learning. Secondly, HypCD (Liu et al., 2025a) explored the use of hyperbolic geometry for GCD. They proposed hyperbolic variants to the original GCD method (Vaze et al., 2022a), SimGCD (Wen et al., 2023), and SelEx (Rastegar et al., 2024), and trained using both angular and distance based contrastive losses. Through all their experiments they

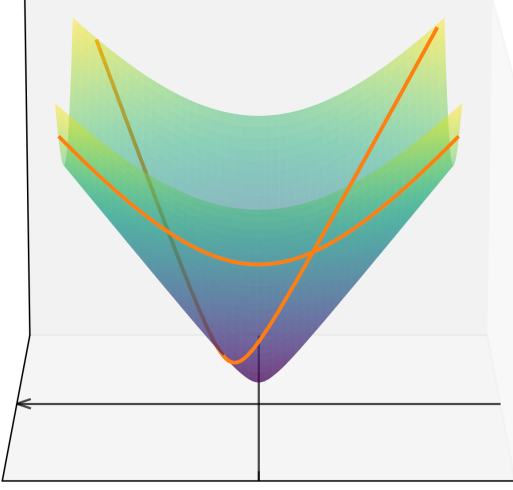


Figure 2: The Lorentz Hyperboloid model \mathbb{H}_1^2 as the upper sheet of a hyperboloid. Shown also are geodesics in this model.

showed clear improvements over the Euclidean variants on standard benchmarks such as the Semantic Shift Benchmark (Vaze et al., 2022b).

However, while the HypCD work considers hyperbolic representation learning and parametric classification, the non-parametric clustering approaches are all applied in Euclidean geometry. Therefore, we investigate in depth the effect of performing K-Means clustering in hyperbolic space.

3 HYPERBOLIC GEOMETRY

Hyperbolic geometry can be represented using different models, with each their own properties. The two models used in this paper are the Lorentz Hyperboloid Model (Desai et al., 2023; Ratcliffe et al., 1994) for representation learning, and the Klein Model (Mao et al., 2024; Ratcliffe et al., 1994) for its closed form Einstein Midpoint.

3.1 The Lorentz Hyperboloid Model

Hyperbolic geometry in the Lorentz Hyperboloid model \mathbb{H}_κ^n is represented as the upper sheet of a hyperboloid in \mathbb{R}^{n+1} :

$$\mathbb{H}_\kappa^n = \left\{ \mathbf{x} \in \mathbb{R}^{n+1} \mid \langle \mathbf{x}, \mathbf{x} \rangle_{\mathbb{L}} = -\frac{1}{\kappa}, x_0 > 0 \right\} \quad (1)$$

Where $\langle \mathbf{x}, \mathbf{x} \rangle_{\mathbb{L}} = -x_0^2 + x_1^2 + \dots + x_n^2$ is the Lorentz inner product and $\kappa = -c$, where c is the curvature.

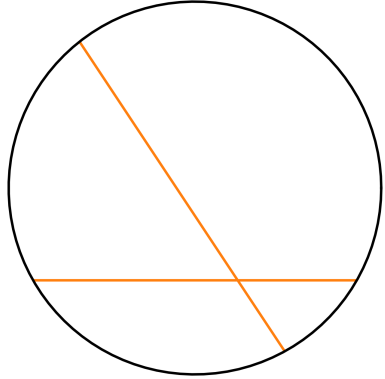


Figure 3: The Klein model \mathbb{K}_1^2 as a circle with radius under $1/\kappa$. This model is the projection of the Lorentz Hyperboloid \mathbb{H}_1^2 from Figure 2, which shows how the geodesics project into straight lines.

Figure 2 shows \mathbb{H}_1^2 as an example. Borrowing from special relativity theory, a point in the Lorentz Hyperboloid model can be written as $\mathbf{x}_{\mathbb{H}} = [x_{time}; \mathbf{x}_{space}]$. Representing the axis of symmetry of the hyperboloid as the time dimension and allowing the Lorentz inner product to be simplified to:

$$\langle \mathbf{x}_{\mathbb{H}}, \mathbf{y}_{\mathbb{H}} \rangle_{\mathbb{L}} = -x_{time}y_{time} + \langle \mathbf{x}_{space}, \mathbf{y}_{space} \rangle \quad (2)$$

Where, $\langle \mathbf{x}, \mathbf{y} \rangle$ is the Euclidean dot product. Additionally, due to the constraint $\langle \mathbf{x}, \mathbf{x} \rangle_{\mathbb{L}} = -\frac{1}{\kappa}$ it is possible to calculate the value of x_{time} from \mathbf{x}_{space} :

$$x_{time} = \sqrt{1/\kappa + \langle \mathbf{x}_{space}, \mathbf{x}_{space} \rangle} \quad (3)$$

Furthermore, the distance between two points on the Lorentz Hyperboloid is given as:

$$d_{\mathbb{H}}(\mathbf{x}, \mathbf{y}) = \sqrt{\frac{1}{\kappa} \cosh^{-1}(-\kappa \langle \mathbf{x}, \mathbf{y} \rangle_{\mathbb{L}})} \quad (4)$$

And lastly, the exponential map can be used to map vectors from the Euclidean tangent space to the Lorentz Hyperboloid:

$$\mathbf{x}_{space} = \text{exp}_m(\mathbf{v}) = \frac{\sinh(\sqrt{\kappa} \|\mathbf{v}\|)}{\sqrt{\kappa} \|\mathbf{v}\|} \mathbf{v} \quad (5)$$

Where $\mathbf{v} \in \mathbb{R}^n$ is a point in Euclidean geometry, and $\|\mathbf{v}\|$ is the L2 norm. While the exponential map only calculates \mathbf{x}_{space} , Equation 3 can be used to find x_{time} .

3.2 The Klein Model

The Klein model is constructed by projecting the Lorentz Hyperboloid in \mathbb{R}^{n+1} into an n-dimensional

hypersphere of radius $1/\sqrt{\kappa}$ with center at the origo of the hyperboloid $\mathbf{O}_{\mathbb{L}} = [1/\sqrt{\kappa}; \mathbf{0}]$:

$$\mathbf{x}_{\mathbb{K}} = \frac{\mathbf{x}_{space}}{\sqrt{\kappa}x_{time}} \quad (6)$$

Where $\mathbf{x}_{\mathbb{K}}$ is a point in the Klein model. This construction makes it isometric to the Lorentz Hyperboloid Model. Being a hypersphere, the set of points in the Klein Model are:

$$\mathbb{K}_{\kappa}^n = \left\{ \mathbf{x} \in \mathbb{R}^n; \|\mathbf{x}\|^2 < \frac{1}{\kappa} \right\} \quad (7)$$

A special property of the Klein model is that its geodesics are straight lines in \mathbb{R}^n , as can be seen in Figure 3. This makes it straightforward to define a midpoint in the Klein model (Mettes et al., 2024), with one such midpoint being the Einstein Midpoint:

$$\mu_{\mathbb{K}} = \frac{\sum_{i=1} \gamma_i \mathbf{x}_{\mathbb{K},i}}{\sum_{i=1} \gamma_i} \quad (8)$$

Where γ_i are the Lorentz factors:

$$\gamma_i = \frac{1}{\sqrt{1 - \kappa \|\mathbf{x}_{\mathbb{K},i}\|^2}} \quad (9)$$

Lastly, the exponential map in the Klein model is:

$$\mathbf{x}_{\mathbb{K}} = \text{expm}(\mathbf{v}) = \frac{\tanh(\sqrt{\kappa} \|\mathbf{v}\|)}{\sqrt{\kappa} \|\mathbf{v}\|} \mathbf{v}, \mathbf{v} \in \mathbb{R}^n \quad (10)$$

4 HYPERBOLIC K-MEANS

The K-Means clustering algorithm requires a distance function and a centroid. In Euclidean K-Means the Euclidean distance and the arithmetic mean are used. However, in order to use K-Means in hyperbolic geometry, an equivalent distance function and centroid are needed.

For points on the Lorentz Hyperboloid, the distance function $d_{\mathbb{H}}$ from Equation 4 can be used. As for the centroid, one option is the Einstein Midpoint in the Klein model found in Equation 8, which would require mapping between the Lorentz Hyperboloid and Klein Hypersphere. Another option is the Lorentz Centroid (Law et al., 2019) computed directly from points on the Lorentz Hyperboloid:

$$\mu_{\mathbb{H}} = \frac{1}{\sqrt{\kappa}} \frac{\sum_{i=1} w_i \mathbf{x}_{\mathbb{H},i}}{\|\sum_{i=1} w_i \mathbf{x}_{\mathbb{H},i}\|_{\mathbb{L}}} \quad (11)$$

Where w_i are arbitrary sample weights and $\|\mathbf{x}\|_{\mathbb{L}} = \sqrt{\langle \mathbf{x}, \mathbf{x} \rangle_{\mathbb{L}}}$ is the Lorentz norm. The Lorentz Centroid minimizes the squared Lorentzian distance between the centroid and all points:

$$d_{\mathbb{L}}^2(\mu, \mathbf{x}) = \|\mu - \mathbf{x}\|_{\mathbb{L}}^2 = -2 \frac{1}{\sqrt{\kappa}} - 2 \langle \mu, \mathbf{x} \rangle_{\mathbb{L}} \quad (12)$$

Which does not trivially translate to minimizing the squared Lorentz Hyperboloid distance:

$$d_{\mathbb{H}}^2(\mu, \mathbf{x}) = \frac{1}{\kappa} \cosh^{-1}(-\kappa \langle \mu, \mathbf{x} \rangle_{\mathbb{L}}) \quad (13)$$

making it uncertain if it can be used as a centroid. However, it is possible to prove that the Einstein Midpoint is the projection of the Lorentz Centroid from the Lorentz Hyperboloid to the Klein Hypersphere:

Lemma 1. *The function mapping points from the Klein model to points on the Lorentz Hyperboloid is:*

$$\pi_{\mathbb{K} \rightarrow \mathbb{H}}(\mathbf{x}_{\mathbb{K}}) = \frac{1}{\sqrt{\kappa - \kappa^2 \|\mathbf{x}_{\mathbb{K}}\|^2}} [1; \sqrt{\kappa} \mathbf{x}_{\mathbb{K}}] \quad (14)$$

Corollary 1.1. *The Lorentz factors in the Einstein Midpoint can be written as:*

$$\gamma_i = \frac{\sqrt{\kappa}}{\sqrt{\kappa - \kappa^2 \|\mathbf{x}_{\mathbb{K}}\|^2}} = \sqrt{\kappa} x_{time} \quad (15)$$

The proof for Lemma 1 can be found in the appendix.

Theorem 1. *The Einstein Midpoint $\mu_{\mathbb{K}}$ can be found by passing the Lorentz Centroid $\mu_{\mathbb{H}}$ through the map $\pi_{\mathbb{H} \rightarrow \mathbb{K}}$:*

$$\mu_{\mathbb{K}} = \pi_{\mathbb{H} \rightarrow \mathbb{K}}(\mu_{\mathbb{H}}) \quad (16)$$

Proof. The Lorentz centroid can be split into its separate space and time components as:

$$\mu_{time} = \frac{1}{\sqrt{\kappa}} \frac{\sum_{i=1} w_i x_{time}}{\|\sum_{i=1} w_i \mathbf{x}_{\mathbb{H},i}\|_{\mathbb{L}}} \quad (17)$$

$$\mu_{space} = \frac{1}{\sqrt{\kappa}} \frac{\sum_{i=1} w_i \mathbf{x}_{space,i}}{\|\sum_{i=1} w_i \mathbf{x}_{\mathbb{H},i}\|_{\mathbb{L}}} \quad (18)$$

Using these components the mapping $\pi_{\mathbb{H} \rightarrow \mathbb{K}}(\mu_{\mathbb{H}})$ evaluates to:

$$\pi_{\mathbb{H} \rightarrow \mathbb{K}}(\mu_{\mathbb{H}}) = \frac{\mu_{space}}{\sqrt{\kappa} \mu_{time}} = \frac{\sum_{i=1} w_i \mathbf{x}_{space,i}}{\sqrt{\kappa} \sum_{i=1} w_i x_{time}} \quad (19)$$

Which is equal to the Einstein Midpoint if $w_i = 1, \forall i$:

$$\mu_{\mathbb{K}} = \frac{\sum_{i=1} \gamma_i \mathbf{x}_{\mathbb{K},i}}{\sum_{i=1} \gamma_i} \quad (20)$$

$$\mu_{\mathbb{K}} = \frac{\sum_{i=1} \sqrt{\kappa} x_{time,i} \frac{\mathbf{x}_{space,i}}{\sqrt{\kappa} x_{time,i}}}{\sum_{i=1} \sqrt{\kappa} x_{time,i}} \quad (21)$$

$$\mu_{\mathbb{K}} = \frac{\sum_{i=1} \mathbf{x}_{space,i}}{\sqrt{\kappa} \sum_{i=1} x_{time}} = \pi_{\mathbb{H} \rightarrow \mathbb{K}}(\mu_{\mathbb{H}}) \quad (22)$$

□

With this proof the two choices become one, and the Lorentz Centroid can be used as a centroid for the hyperbolic K-Means algorithm without having to

transform between hyperbolic models. Furthermore, this proof makes it possible to create an equivalent algorithm for the Poincaré model, used in an ablation study in Section 7.1, by utilizing the Einstein Mid-point as a centroid. Figure 1 shows an example of the hyperbolic semi-supervised K-Means algorithm in \mathbb{H}^2_1 .

5 METHOD

5.1 GCD Task Definition

Generalized Category Discovery (GCD) is an open world classification task, where an algorithm has to cluster a dataset with points belonging to either seen or unseen classes. This is achieved by splitting a dataset into two subsets, an unlabeled subset $D_{\mathcal{U}} : \{x_i, y_i\} \in X, Y_{\mathcal{U}}$ and a labeled subset $D_{\mathcal{L}} : \{x_i, y_i\} \in X, Y_{\mathcal{L}}$ where $Y_{\mathcal{L}} \subset Y_{\mathcal{U}}$. The training set includes samples from both $D_{\mathcal{L}}$ and $D_{\mathcal{U}}$, but only labels from $D_{\mathcal{L}}$, resulting in a need for a combination of unsupervised and supervised learning. During testing, the algorithm needs to classify samples belonging to both seen and unseen classes (Vaze et al., 2022a).

5.2 HC-GCD

The Hyperbolic Clustered GCD (HC-GCD) model closely follows the HypCD implementation of the GCD model (Hyp-GCD) by Liu et al. (2025b). The backbone uses a Vision Transformer (ViT) (Dosovitskiy et al., 2020) and a projector head, followed by clipping the norm of the Euclidean embeddings (Guo et al., 2022) and transformation into hyperbolic space using an exponential map. While Hyp-GCD transforms to the Poincaré Hypersphere, HC-GCD transforms to the Lorentz Hyperboloid.

The training procedure also mirrors that of Hyp-GCD, using a combination of distance based and angle based self-supervised and supervised contrastive losses. Given the contrastive score between two samples $\sigma(i, \mathbf{y}_{\mathbb{H}})$, where i is the index of the sample, and \mathbf{y} is the positive sample. The self-supervised and supervised contrastive losses are:

$$\mathcal{L}_{\sigma,i}^u = -\log(\sigma(i, \mathbf{z}'_{\mathbb{H},i})) \quad (23)$$

$$\mathcal{L}_{\sigma,i}^s = -\frac{1}{|\mathcal{N}(i)|} \sum_{q \in \mathcal{N}(i)} \log(\sigma(i, \mathbf{z}_{\mathbb{H},q})) \quad (24)$$

Where $\mathbf{z}_{\mathbb{H},i}$ and $\mathbf{z}'_{\mathbb{H},i}$ are embeddings from two views, where each view is an augmentation of sample i , and $\mathcal{N}(i)$ is a set of indices belonging to the same class as index i . For the distance based contrastive loss,

the contrastive score uses the negative hyperbolic distance as a similarity metric:

$$\sigma_D(i, \mathbf{y}) = \frac{\exp(-d_{\mathbb{H}}(\mathbf{z}_{\mathbb{H},i}, \mathbf{y})/\tau)}{\sum_n \mathbf{1}_{[n \neq i]} \exp(-d_{\mathbb{H}}(\mathbf{z}_{\mathbb{H},i}, \mathbf{z}_{\mathbb{H},n})/\tau)} \quad (25)$$

Where τ is a temperature constant and $\mathbf{1}_{[n \neq i]}$ is an indicator function that evaluates to 1 if and only if $n \neq i$.

For the angle based losses the exterior angle from MERU (Desai et al., 2023) is utilized:

$$\text{ext}(\mathbf{x}, \mathbf{y}) = \cos^{-1} \left(\frac{y_{time} + x_{time} \kappa \langle \mathbf{x}, \mathbf{y} \rangle_{\mathbb{L}}}{\|\mathbf{x}_{space}\| \sqrt{(\kappa \langle \mathbf{x}, \mathbf{y} \rangle_{\mathbb{L}})^2 - 1}} \right) \quad (26)$$

$$\sigma_A(i, \mathbf{y}) = \frac{\exp(\text{ext}(\mathbf{z}_{\mathbb{H},i}, \mathbf{y})/\tau)}{\sum_n \mathbf{1}_{[n \neq i]} \exp(\text{ext}(\mathbf{z}_{\mathbb{H},i}, \mathbf{z}_{\mathbb{H},n})/\tau)} \quad (27)$$

The total training loss is a weighted combination of all four losses:

$$\mathcal{L}^s = ((1 - \alpha) \mathcal{L}_{\sigma_D}^s + \alpha \mathcal{L}_{\sigma_A}^s) \quad (28)$$

$$\mathcal{L}^u = ((1 - \alpha) \mathcal{L}_{\sigma_D}^u + \alpha \mathcal{L}_{\sigma_A}^u) \quad (29)$$

$$\mathcal{L} = (1 - \lambda) \mathcal{L}^s + \lambda \mathcal{L}^u \quad (30)$$

With λ being the weighting hyperparameter between self-supervised and supervised contrastive loss, and α being the weighting hyperparameter between distance and angle-based losses. Similar to Hyp-GCD the α weight is linearly decayed from 1 to 0 as training progresses.

After finished training, the hyperbolic K-Means algorithm is used to cluster the embeddings in the Lorentz Hyperboloid present by the model. Figure 4 shows the overall HC-GCD model pipeline.

6 EXPERIMENTAL DESIGN

The experiments were carried on the Semantic Shift Benchmark (SSB) datasets (Vaze et al., 2022b), namely CUB (Wah et al., 2011), Stanford Cars (Krause et al., 2013) and FGVC-Aircraft (Maji et al., 2013). Following the original GCD setup, half of the classes are assigned as seen classes $Y_{\mathcal{L}}$. Thereafter, the labeled dataset $D_{\mathcal{L}}$ is comprised from 50% of the samples belonging to the seen classes. The remaining samples from both seen and unseen classes create the unlabeled dataset $D_{\mathcal{U}}$ (Vaze et al., 2022a).

The HC-GCD model uses a ViT-B14 (Dosovitskiy et al., 2020) pre-trained with DINOv2 (Oquab et al., 2024) as baseline followed by a projection head comprised of 4 linear layers and GELU (Hendrycks and Gimpel, 2023) activations according to this setup:

$$\mathbb{R}^I \xrightarrow{\text{GELU}} \mathbb{R}^{2048} \xrightarrow{\text{GELU}} \mathbb{R}^{2048} \xrightarrow{\text{GELU}} \mathbb{R}^{256} \rightarrow \mathbb{R}^{256} \quad (31)$$

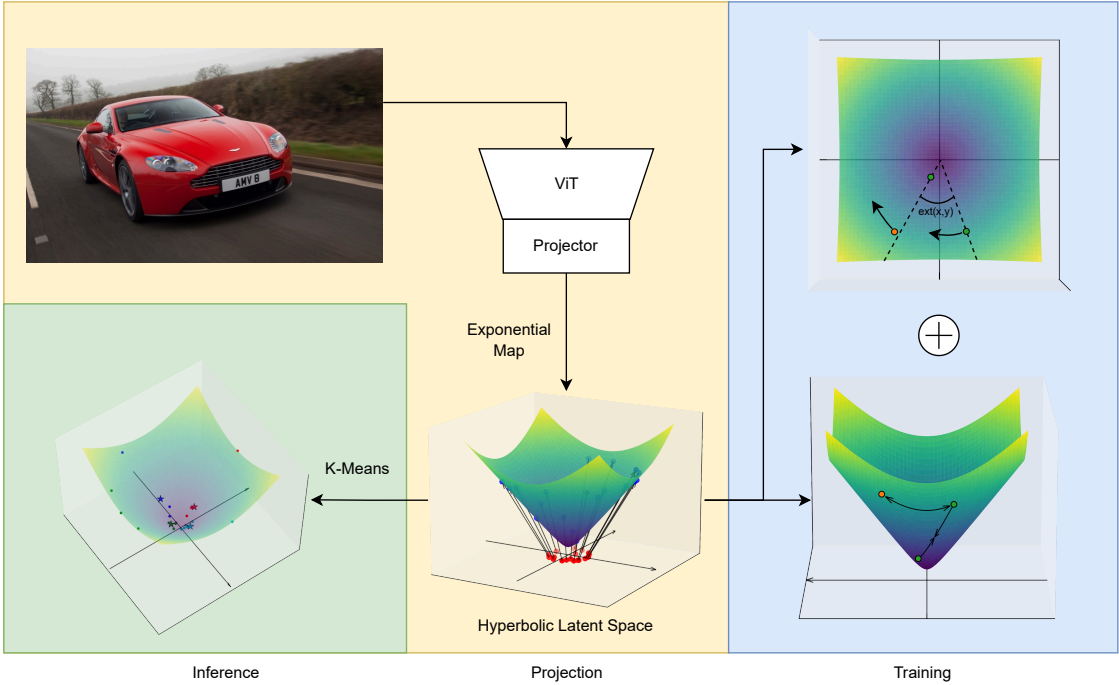


Figure 4: Full pipeline of HC-GCD. Training uses combination of distance and angle based contrastive loss. After training is finished, a hyperbolic semi-supervised K-Means algorithm is used for clustering the embeddings in the Lorentz Hyperboloid.

Where I is the input dimension for embeddings from the ViT. The Euclidean embeddings outputted by the projection head are then clipped to a norm of 2.3. These clipped embeddings are then transformed to the Lorentz Hyperboloid with a fixed curvature of $c = -0.05$ using the exponential map. These two values are chosen because they were shown to perform best for the SSB datasets in the HypCD paper (Liu et al., 2025b)

During training, gradient clipping is used to avoid exploding gradients. The gradients are clipped to a max absolute value of 1.0, then the gradients are scaled to have a max absolute average of 0.25. Furthermore, a cosine annealing scheduler is used, with a maximum learning rate of 0.1 and a minimum of 0.0001 with a SGD optimizer.

For the losses a temperature value of $\tau = 0.07$ is used and the weight factor α is linearly decayed from 1 to 0, while the other weight factor is $\lambda = 0.35$. The model is trained with a batch size of 128 and for 200 epochs and all models are trained on an Nvidia L40s GPU.

The model with the lowest loss is clustered using both hyperbolic K-Means and Euclidean K-Means. During Euclidean evaluation the projection head is removed, and embeddings directly from the ViT are clustered. The results from the K-Means clustering

are then evaluated using clustering accuracy, which was defined by Vaze et al. (Vaze et al., 2022a). Three accuracy metrics are provided, "All" accuracy calculated using all classes, "Old" accuracy calculated only using seen classes and "New" accuracy calculated only using unseen classes. The full training set is used for clustering, while accuracy is evaluated on only the unlabeled training set as per convention within the GCD field (Vaze et al., 2022a; Liu et al., 2025a; Wen et al., 2023).

7 RESULTS

To compare our results, we trained and evaluated Hyp-GCD locally as a baseline. Table 1 shows the mean accuracy from three different seeds. HC-GCD outperforms in two out of three datasets showing potential in using the Lorentz Hyperboloid model for the GCD task. Furthermore, using the hyperbolic K-Means algorithm leads to improvement on almost all metrics, showing its superiority to Euclidean K-Means when training in the Lorentz Hyperboloid model of hyperbolic geometry.

Table 1 also shows the standard deviation of the reported accuracies. This table shows improved train-

Table 1: Mean and standard deviation of the accuracy of the GCD models on the fine-grained SSB datasets. Lorentz contrastive training refers to HC-GCD while Poincaré refers to Hyp-GCD. For the HC-GCD, performance is reported using both the Euclidean and hyperbolic K-Means algorithms. The highest mean accuracy for each column is highlighted in bold, while the second highest is underlined, while the equivalent is done for the lowest standard deviations.

Contrastive Training	K-Means Algorithm	CUB			Stanford Cars			FGVC-Aircraft		
		All	Old	New	All	Old	New	All	Old	New
Mean (Higher is Better)										
Lorentz	Lorentz	71.70	76.34	69.38	73.69	82.41	69.49	61.90	61.85	61.93
Lorentz	Euclidean	70.22	70.22	<u>70.22</u>	<u>70.74</u>	<u>79.09</u>	<u>66.71</u>	<u>61.31</u>	64.31	<u>59.81</u>
Poincaré	Euclidean	<u>71.52</u>	<u>72.56</u>	71.00	68.31	75.46	64.85	59.36	59.38	59.34
Standard Deviation (Lower is Better)										
Lorentz	Lorentz	00.55	<u>00.93</u>	01.24	00.37	00.57	00.71	<u>02.49</u>	04.04	01.79
Lorentz	Euclidean	<u>01.29</u>	00.74	<u>01.91</u>	<u>00.81</u>	00.90	<u>00.78</u>	02.65	<u>02.56</u>	02.69
Poincaré	Euclidean	02.06	01.36	02.62	01.25	<u>00.61</u>	01.63	02.36	02.49	<u>02.30</u>

ing stability when using the Lorentz Hyperboloid model, as accuracies across seeds are more consistent.

7.1 Ablations

Euclidean Clipping Guo et al. (2022) show that clipping the Euclidean embeddings leads to improved performance on models trained in the Poincaré Hypersphere, as unclipped embeddings lead to vanishing gradient problems. However, this does not necessarily apply to models trained in the Lorentz Hyperboloid. Furthermore, Desai et al. (2023) do not utilize embedding clipping when training MERU. Therefore, an ablation study is carried to investigate the impact of using clipped embeddings when training in the Lorentz Hyperboloid.

Table 2 shows the results of this ablation. These results show that the performance from using embedding clipping is dataset dependant, as tests on FGVC-Aircraft gain an accuracy improvement when clipping is not used. Furthermore, a pattern can be seen with the old and new accuracy, as removing embedding clipping leads to increased accuracy on old classes, and a decreased accuracy on new classes most of the times.

ViT with Registers The code provided by Liu et al. (2025a) for their Hyp-GCD model differed from the original GCD model in two ways:

- The ViT model utilizes registers, following the setup by Dariset et al. (2024).
- The projection MLP is missing the last layer, making it similar to the one used in SimGCD by Wen et al. (2023):

$$\mathbb{R}^I \xrightarrow{\text{GELU}} \mathbb{R}^{2048} \xrightarrow{\text{GELU}} \mathbb{R}^{2048} \xrightarrow{\text{GELU}} \mathbb{R}^{256} \quad (32)$$

Therefore, an ablation study is performed to evaluate the impact of these changes on the HC-GCD model. Table 3 compares the results from the original setup, and the setup using ViT with registers. It can be seen that the Hyp-GCD training setup gains accuracy in all datasets when ViT with registers is used, especially with the Stanford Cars and FGVC-Aircraft datasets. Lorentz training also benefits from using ViT with registers, however, it is not the case in all datasets, as CUB performs better without registers. Regardless, Lorentz training benefits from using the hyperbolic K-Means algorithm regardless of the backbone used.

Consistency Across Label Granularity A key motivation for using hyperbolic geometry is that the space more naturally encodes hierachal structures. We investigate this by varying the label granularity and measuring the number of elements in the predicted clusters which belong to ground truth labels. We determine this using the FGVC Aircraft dataset, constructing coarse to fine-grained labels by using the Manufacturer, Family, and Variant labels for data points. The Homogeneity (Rosenberg and Hirschberg, 2007) metric is used to quantify the clustering performance, as shown in Table 4. We find that HC-GCD generates more consistent clusters across all label granularities, outperforming Hyp-GCD by several percentage points. We also find that performing K-Means in hyperbolic space leads to the best performance across all granularity levels, indicating a clear benefit of clustering in hyperbolic space.

Hyperbolic K-Means in Poincaré An ablation is devised to test the performance of performing K-Means on hyperbolic embeddings from the Hyp-GCD

Table 2: Mean accuracy of the HC-GCD models when trained with a Euclidean clipping of $r = 2.3$ and without any Euclidean clipping. The highest accuracy for each column is highlighted in bold, while the second highest is underlined.

Euclidean Clipping	K-Means Algorithm	CUB			Stanford Cars			FGVC-Aircraft		
		All	Old	New	All	Old	New	All	Old	New
✓	Lorentz	71.70	76.34	69.38	73.69	82.41	69.49	61.90	61.85	61.93
✗	Lorentz	68.88	<u>73.34</u>	66.66	70.20	84.69	63.20	64.72	75.17	59.59
✓	Euclidean	<u>70.22</u>	70.22	70.22	<u>70.74</u>	79.09	<u>66.71</u>	61.31	64.31	59.81
✗	Euclidean	69.28	71.16	68.34	68.77	80.19	63.25	<u>64.18</u>	<u>72.15</u>	<u>60.20</u>

Table 3: Mean accuracy of models trained on a ViT with registers backbone and a projector without its last layer. Lorentz contrastive training refers to HC-GCD while Poincaré refers to Hyp-GCD. Percent difference with models trained without registers and with the last layer of the projector present are reported under each result. The highest accuracy for each column is highlighted in bold, while the second highest is underlined.

Contrastive Training	K-Means Algorithm	CUB			Stanford Cars			FGVC-Aircraft		
		All	Old	New	All	Old	New	All	Old	New
Lorentz	Lorentz	<u>71.59</u>	77.65	68.56	74.79	<u>81.39</u>	71.60	63.08	<u>65.75</u>	61.74
		(-0.11)	(+1.31)	(-0.82)	(+1.10)	(-1.02)	(+1.11)	(+1.18)	(+3.90)	(-0.19)
Lorentz	Euclidean	69.27	69.05	<u>69.38</u>	<u>73.46</u>	80.29	<u>70.17</u>	<u>63.12</u>	61.53	<u>63.91</u>
		(-0.95)	(-1.17)	(-0.84)	(+2.72)	(+1.20)	(+3.46)	(+1.81)	(-2.78)	(+4.10)
Poincaré	Euclidean	72.35	<u>72.31</u>	72.37	72.66	81.51	68.38	64.92	65.95	64.40
		(+0.83)	(-0.25)	(+1.37)	(+4.35)	(+6.05)	(+3.53)	(+5.56)	(+6.57)	(+5.06)

Table 4: Mean homogeneity of the GCD models on the FGVC Aircraft dataset when varying the ground truth label granularity. Lorentz contrastive training refers to HC-GCD while Poincaré refers to Hyp-GCD. The highest homogeneity for each column is highlighted in bold, while the second highest is underlined.

Contrastive Training	K-Means Algorithm	FGVC-Aircraft Labels		
		Manufacturer	Family	Variant
Lorentz	Lorentz	90.46	89.09	82.48
Lorentz	Euclidean	<u>89.99</u>	<u>88.62</u>	<u>82.41</u>
Poincaré	Euclidean	87.14	85.78	80.09

model. To achieve that, a hyperbolic K-Means algorithm for the Poincaré model is used based on the Poincaré distance and the Einstein Midpoint as a centroid. To calculate the Einstein Midpoint, the embeddings in the Poincaré model are transformed to the Klein model, then the calculated midpoint is transformed back to the Poincaré model. This is chosen due to the fact that there are no closed form midpoints in the Poincaré model.

It is possible to compare the hyperbolic K-Means between the Lorentz Hyperboloid model and the Poincaré model due to the distance and centroid being equivalent. The distance functions are equivalent due to the two models being isometric (Ratcliffe et al., 1994), and the centroids are equivalent due to the Einstein Midpoint corresponding to the Lorentz Centroid as per Theorem 1.

We find that clustering in Poincaré space results in close to zero accuracy on all datasets. Upon further inspection we discovered that all samples were always

assigned to a single centroid. Therefore, we conclude that further work is needed in order for K-Means in Poincaré to be made feasible.

8 LIMITATIONS

In this paper we have demonstrated the feasibility and benefits of performing clustering in hyperbolic space. However, our work is not without limitations. We specifically highlight two key limitations. Firstly, our work is missing an adaptation of leading non-parametric methods within the GCD field, such as Hyp-SelEx. These were excluded as we focused on isolating the effect of hyperbolic clustering, with no bells or whistles. Secondly, we have not demonstrated the effectiveness of hyperbolic clustering in the Poincaré hyperbolic space. This warrants a deeper future study into the feasibility of hyperbolic clustering across different hyperbolic geometry models.

9 CONCLUSION

Throughout this paper we have investigated whether using hyperbolic representation learning and clustering in the Lorentz Hyperboloid model is beneficial for the GCD task. This is due to the fact that previous hyperbolic methods choose to remove the hyperbolic exponential map during inference and cluster directly

on Euclidean embeddings, which may lead to misrepresentation of the learned hierarchical structures. To that end, we adapt the K-Means algorithm to hyperbolic geometry, and adapt the original GCD model by Vaze et al. (2022a) creating the Hyperbolic Clustered GCD (HC-GCD) method. We test our method using both hyperbolic and Euclidean K-Means, while comparing to the Hyp-GCD model by Liu et al, which trains in the Poincaré model of hyperbolic geometry.

Our results show that using the Lorentz Hyperboloid model for representation learning performs on par with Hyp-GCD, while also showing that hyperbolic clustering is necessary for improved performance when training in the Lorentz Hyperboloid model. Furthermore, our ablations showed that clustering directly in hyperbolic space leads to more consistent predictions across label granularity, as the model trained in the Lorentz Hyperboloid and clustered with hyperbolic K-Means achieved the highest homogeneity on all FGVC-Aircraft label classes.

ACKNOWLEDGMENTS

This work was supported by the Pioneer Centre for AI (DNRF grant number P1).

REFERENCES

Atigh, M. G., Schoep, J., Acar, E., van Noord, N., and Mettes, P. (2022). Hyperbolic image segmentation. In *Proceedings of the IEEE/CVF Conference on Computer Vision and Pattern Recognition (CVPR)*, pages 4453–4462.

Dariset, T., Oquab, M., Mairal, J., and Bojanowski, P. (2024). Vision transformers need registers.

Desai, K., Nickel, M., Rajpurohit, T., Johnson, J., and Vedantam, S. R. (2023). Hyperbolic image-text representations. In Krause, A., Brunskill, E., Cho, K., Engelhardt, B., Sabato, S., and Scarlett, J., editors, *Proceedings of the 40th International Conference on Machine Learning*, volume 202 of *Proceedings of Machine Learning Research*, pages 7694–7731. PMLR.

Dosovitskiy, A., Beyer, L., Kolesnikov, A., Weissenborn, D., Zhai, X., Unterthiner, T., Dehghani, M., Minderer, M., Heigold, G., Gelly, S., Uszkoreit, J., and Houlsby, N. (2020). An image is worth 16x16 words: Transformers for image recognition at scale. *CoRR*, abs/2010.11929.

Ge, S., Mishra, S., Kornblith, S., Li, C.-L., and Jacobs, D. (2023). Hyperbolic contrastive learning for visual representations beyond objects. In *Proceedings of the IEEE/CVF Conference on Computer Vision and Pattern Recognition (CVPR)*, pages 6840–6849.

Ghadimi Atigh, M., Keller-Ressel, M., and Mettes, P. (2021). Hyperbolic busemann learning with ideal prototypes. In Ranzato, M., Beygelzimer, A., Dauphin, Y., Liang, P., and Vaughan, J. W., editors, *Advances in Neural Information Processing Systems*, volume 34, pages 103–115. Curran Associates, Inc.

Gromov, M. (1987). *Hyperbolic Groups*, pages 75–263. Springer New York, New York, NY.

Guo, Y., Wang, X., Chen, Y., and Yu, S. X. (2022). Clipped hyperbolic classifiers are super-hyperbolic classifiers. In *Proceedings of the IEEE/CVF Conference on Computer Vision and Pattern Recognition (CVPR)*, pages 11–20.

He, Z., Liu, Y., and Han, K. (2025a). Category discovery: An open-world perspective.

He, Z., Liu, Y., and Han, K. (2025b). Seal: Semantic-aware hierarchical learning for generalized category discovery. In *Conference on Neural Information Processing Systems (NeurIPS)*.

Hendrycks, D. and Gimpel, K. (2023). Gaussian error linear units (gelus).

Hsu, J., Gu, J., Wu, G., Chiu, W., and Yeung, S. (2021). Capturing implicit hierarchical structure in 3d biomedical images with self-supervised hyperbolic representations. In Ranzato, M., Beygelzimer, A., Dauphin, Y., Liang, P., and Vaughan, J. W., editors, *Advances in Neural Information Processing Systems*, volume 34, pages 5112–5123. Curran Associates, Inc.

Krause, J., Stark, M., Deng, J., and Fei-Fei, L. (2013). 3d object representations for fine-grained categorization. In *Proceedings of the IEEE International Conference on Computer Vision (ICCV) Workshops*.

Krioukov, D., Papadopoulos, F., Kitsak, M., Vahdat, A., and Boguñá, M. (2010). Hyperbolic geometry of complex networks. *Phys. Rev. E*, 82:036106.

Law, M., Liao, R., Snell, J., and Zemel, R. (2019). Lorentzian distance learning for hyperbolic representations. In Chaudhuri, K. and Salakhutdinov, R., editors, *Proceedings of the 36th International Conference on Machine Learning*, volume 97 of *Proceedings of Machine Learning Research*, pages 3672–3681. PMLR.

Leimeister, M. and Wilson, B. J. (2018). Skip-gram word embeddings in hyperbolic space. *CoRR*, abs/1809.01498.

Liu, Y., He, Z., and Han, K. (2025a). Hyperbolic category discovery. In *Proceedings of the IEEE/CVF Conference on Computer Vision and Pattern Recognition (CVPR)*.

Liu, Y., He, Z., and Han, K. (2025b). Hyperbolic category discovery. In *Proceedings of the IEEE/CVF Conference on Computer Vision and Pattern Recognition (CVPR)*, pages 9891–9900.

Maji, S., Rahtu, E., Kannala, J., Blaschko, M., and Vedaldi, A. (2013). Fine-grained visual classification of aircraft. *arXiv preprint arXiv:1306.5151*.

Mao, Y., Gu, J., Werner, M. C., and Zou, D. (2024). Klein model for hyperbolic neural networks.

Mettes, P., Ghadimi Atigh, M., Keller-Ressel, M., Gu, J., and Yeung, S. (2024). Hyperbolic deep learning in computer vision: A survey. *International Journal of Computer Vision*, 132(9):3484–3508.

Mikolov, T., Chen, K., Corrado, G., and Dean, J. (2013). Efficient estimation of word representations in vector space.

Quab, M., Darzet, T., Moutakanni, T., Vo, H., Szafraniec, M., Khalidov, V., Fernandez, P., Haziza, D., Massa, F., El-Nouby, A., Assran, M., Ballas, N., Galuba, W., Howes, R., Huang, P.-Y., Li, S.-W., Misra, I., Rabbat, M., Sharma, V., Synnaeve, G., Xu, H., Jegou, H., Mairal, J., Labatut, P., Joulin, A., and Bojanowski, P. (2024). Dinnov2: Learning robust visual features without supervision.

Peng, W., Varanka, T., Mostafa, A., Shi, H., and Zhao, G. (2022). Hyperbolic deep neural networks: A survey. *IEEE Transactions on Pattern Analysis and Machine Intelligence*, 44(12):10023–10044.

Rastegar, S., Doughty, H., and Snoek, C. (2023). Learn to categorize or categorize to learn? self-coding for generalized category discovery. In *Thirty-seventh Conference on Neural Information Processing Systems*.

Rastegar, S., Salehi, M., Asano, Y. M., Doughty, H., and Snoek, C. G. M. (2024). Selex: Self-expertise in fine-grained generalized category discovery. In *European Conference on Computer Vision*.

Ratcliffe, J. G., Axler, S., and Ribet, K. A. (1994). *Foundations of hyperbolic manifolds*, volume 149. Springer.

Rathore, V., Gupta, D., and Banerjee, B. (2025). Hidisc: A hyperbolic framework for domain generalization with generalized category discovery. In *Conference on Neural Information Processing Systems (NeurIPS)*.

Rosenberg, A. and Hirschberg, J. (2007). V-measure: A conditional entropy-based external cluster evaluation measure. In *Proceedings of the 2007 Joint Conference on Empirical Methods in Natural Language Processing and Computational Natural Language Learning (EMNLP-CoNLL)*, pages 410–420, Prague, Czech Republic. Association for Computational Linguistics.

Suris, D., Liu, R., and Vondrick, C. (2021). Learning the predictability of the future. In *Proceedings of the IEEE/CVF Conference on Computer Vision and Pattern Recognition (CVPR)*, pages 12607–12617.

van Spengler, M., Berkhout, E., and Mettes, P. (2023). Poincaré ResNet. In *2023 IEEE/CVF International Conference on Computer Vision (ICCV)*, pages 5396–5405, Los Alamitos, CA, USA. IEEE Computer Society.

Vaze, S., Han, K., Vedaldi, A., and Zisserman, A. (2022a). Generalized category discovery. In *Proceedings of the IEEE/CVF Conference on Computer Vision and Pattern Recognition (CVPR)*, pages 7492–7501.

Vaze, S., Han, K., Vedaldi, A., and Zisserman, A. (2022b). The semantic shift benchmark. In *ICML 2022 Shift Happens Workshop*.

Vaze, S., Vedaldi, A., and Zisserman, A. (2023). No representation rules them all in category discovery. In *Advances in Neural Information Processing Systems 37*.

Wah, C., Branson, S., Welinder, P., Perona, P., and Belongie, S. (2011). The caltech-ucsd birds-200-2011 dataset.

Wang, H., Vaze, S., and Han, K. (2024). Sptnet: An efficient alternative framework for generalized category discovery with spatial prompt tuning. In *International Conference on Learning Representations (ICLR)*.

Wen, X., Zhao, B., and Qi, X. (2023). Parametric classification for generalized category discovery: A baseline study. In *Proceedings of the IEEE/CVF International Conference on Computer Vision (ICCV)*, pages 16590–16600.

Yun, S., Han, D., Oh, S. J., Chun, S., Choe, J., and Yoo, Y. (2019). Cutmix: Regularization strategy to train strong classifiers with localizable features. In *International Conference on Computer Vision (ICCV)*.

Zhao, B., Wen, X., and Han, K. (2023). Learning semi-supervised gaussian mixture models for generalized category discovery. In *Proceedings of the IEEE/CVF International Conference on Computer Vision (ICCV)*, pages 16623–16633.

APPENDIX

Lemma 1. *The function mapping points from the Klein model to points on the Lorentz Hyperboloid is:*

$$\pi_{\mathbb{K} \rightarrow \mathbb{H}}(\mathbf{x}_{\mathbb{K}}) = \frac{1}{\sqrt{\kappa - \kappa^2 \|\mathbf{x}_{\mathbb{K}}\|^2}} [1; \sqrt{\kappa} \mathbf{x}_{\mathbb{K}}] \quad (33)$$

Proof. Using the property $x_{time} = \sqrt{1/\sqrt{\kappa} + \|\mathbf{x}_{space}\|^2}$, we can rewrite Equation 6, mapping points from the Lorentz Hyperboloid to the Klein model, as:

$$\mathbf{x}_{\mathbb{K}} = \frac{\mathbf{x}_{space}}{\sqrt{\kappa} x_{time}} = \frac{\mathbf{x}_{space}}{\sqrt{\kappa} \sqrt{1/\kappa + \|\mathbf{x}_{space}\|^2}} \quad (34)$$

On the other hand, by rearranging the same mapping function, we get:

$$\mathbf{x}_{space} = \sqrt{\kappa} x_{time} \mathbf{x}_{\mathbb{K}} \quad (35)$$

By replacing \mathbf{x}_{space} in Equation 34 with the value in Equation 35 we get:

$$\mathbf{x}_{\mathbb{K}} = \frac{\sqrt{\kappa} x_{time}}{\sqrt{\kappa} \sqrt{1/\kappa + \|\sqrt{\kappa} x_{time} \mathbf{x}_{\mathbb{K}}\|^2}} \mathbf{x}_{\mathbb{K}} \quad (36)$$

$$\mathbf{x}_{\mathbb{K}} = \frac{x_{time}}{\sqrt{1/\kappa + \kappa x_{time}^2 \|\mathbf{x}_{\mathbb{K}}\|^2}} \mathbf{x}_{\mathbb{K}} \quad (37)$$

Which means that:

$$1 = \frac{x_{time}}{\sqrt{1/\kappa + \kappa x_{time}^2 \|\mathbf{x}_{\mathbb{K}}\|^2}} \quad (38)$$

$$1/\kappa + \kappa x_{time}^2 \|\mathbf{x}_{\mathbb{K}}\|^2 = x_{time}^2 \quad (39)$$

$$1/\kappa = (1 - \kappa \|\mathbf{x}_{\mathbb{K}}\|^2) x_{time}^2 \quad (40)$$

$$\frac{1}{\kappa(1 - \kappa \|\mathbf{x}_{\mathbb{K}}\|^2)} = x_{time}^2 \quad (41)$$

$$\frac{1}{\sqrt{\kappa - \kappa^2 \|\mathbf{x}_{\mathbb{K}}\|^2}} = x_{time} \quad (42)$$

By inserting the value of x_{time} into Equation 35 we get:

$$\mathbf{x}_{space} = \sqrt{\kappa} \frac{1}{\sqrt{\kappa - \kappa^2 \|\mathbf{x}_{\mathbb{K}}\|^2}} \mathbf{x}_{\mathbb{K}} \quad (43)$$

Hence, using the definitions of x_{time} and \mathbf{x}_{space} from Equations 42 and 43 respectively the mapping function becomes:

$$\pi_{\mathbb{K} \rightarrow \mathbb{H}}(\mathbf{x}_{\mathbb{K}}) = \frac{1}{\sqrt{\kappa - \kappa^2 \|\mathbf{x}_{\mathbb{K}}\|^2}} [1; \sqrt{\kappa} \mathbf{x}_{\mathbb{K}}] \quad (44)$$

□